Realizing high-performance Zn-ion batteries by a reduced graphene oxide block layer at room and low temperatures

Jian-Qiu Huang, Xiuyi Lin, Hong Tan, Xiaoqiong Du, Biao Zhang*

Department of Applied Physics, The Hong Kong Polytechnic University, Hung Hom, Hong Kong, PR China.
**Corresponding author. E-mail address: biao.ap.zhang@polyu.edu.hk (Biao Zhang)*

Abstract

Rechargeable aqueous Zn-ion batteries (ZIBs) have attracted great attention due to their cost-effectiveness, high safety, and environmental friendliness. However, some issues associated with poor structural instability of cathode materials and fast self-discharge hinder the further development of ZIBs. Herein, a new configuration is introduced by placing a reduced graphene oxide film as a block layer between the separator and the $V_2O_5 \cdot nH_2O$ cathode. This layer prevents the free diffusion of dissolved active materials to the anode and facilitates the transport of Zn ion and electrons, largely improving the cyclic stability and alleviating the self-discharge. Accordingly, the optimized battery delivers a remarkable capacity of 191 mAh g^{-1} after 500 cycles at 2 A g^{-1}. Moreover, a high capacity of 106 mAh g^{-1} is achieved after 100 cycles at -20 °C. The strategy proposed is expected to be applicable to other electrode systems, thus offering a new approach to circumvent the critical challenges facing aqueous batteries.

Keywords: block layer; dissolution; self-discharge; low temperatures; aqueous Zn-ion

batteries.

1. Introduction

Lithium-ion batteries (LIBs) are considered as the most popular rechargeable battery systems due to their high energy density and stable cyclic performance [1]. Large-scale application of LIBs is partly limited by the safety issues arising from organic electrolytes and the increasing cost. Multivalent (e.g., Mg^{2+}, Zn^{2+}, and Al^{3+}) metal battery is emerging as one of the most promising candidates for new secondary battery systems, providing an attractive opportunity in energy storage research [2]. Among these metals, Zn demonstrates the superiority because of the high theoretical volumetric and gravimetric capacities (5851 mAh mL^{-1} and 820 mAh g^{-1}), the low redox potential of Zn/Zn^{2+} (-0.76 V vs. standard hydrogen electrode, SHE) and low cost of Zn resources [3-4].

Recently, rechargeable aqueous Zn-ion batteries (ZIBs) have attracted extensive attention taking advantages of both the high capacities of Zn anode and the non-flammability, low-cost electrolytes [4-5]. Several promising cathodes have been designed, such as MnO_2 [6-8], Prussian blue analogs [9-10] and vanadium based materials [4, 11-14], which delivers excellent capability in uptaking Zn ions. Nevertheless, the high solubility of active materials in the aqueous electrolyte has

caused a severe problem on the cyclic stability [15]. To address the issue, a few strategies have been proposed, including i) developing electrolyte additives. The addition of $MnSO_4$ in the electrolyte has largely inhibited the dissolution of Mn^{2+} from Mn^{3+} disproportion [4, 15] in the MnO_2 cathode; ii) designing a protective coating layer. Coating of a conductive polymer or carbon on active materials has brought about benefits on both the cyclic life and rate capability [16, 17]; and iii) applying the hybrid organic/aqueous electrolyte to stabilize the structure of $V_2O_5 \cdot nH_2O$ nanowires [18]. These efforts effectively alleviate the shuttle of active materials, and thus significantly improve the cyclic life.

Instead of modifying the electrolyte and electrode materials, we present another approach, which utilizes an interlayer, to prevent the shuttle of active materials. The concept has been adopted in organic Li-sulfur batteries, but its effect on the aqueous ZIBs system has yet been evaluated to the best of our knowledge. A freestanding reduced graphene oxide (rGO) film prepared by self-assembly and thermal reduction is placed between separator and cathode. This strategy can avoid the structure change of active materials when the reduction degree of rGO is controlled. The film functions as a block layer to prevent the migration of dissolved active materials and stabilize them for re-utilization, largely improving the cyclic stability of the battery. Application-wise, the insertion of this block layer has also enabled the ZIBs to be used under low

temperature down to -20 ºC.

2. Experimental

2.1. Preparation of rGO films

GO dispersion was prepared via a modified Hummers method as described in previous work [19, 20]. 50 ml of GO dispersion with a concentration of 2 mg ml^{-1} was poured into a homemade Teflon cell with a size of 100 mm×100 mm, as shown in Fig. 1a. After drying at 60 ℃ for overnight, the GO film was peeled off and thermally reduced at 350, 600 and 1000 ℃ for 1 h in the Ar atmosphere, which is denoted as 350rGO, 600rGO and 1000rGO, respectively. These films were then cut into discs with a diameter of 14 mm and directly used as the block layer.

2.2. Characterization

The morphologies of rGO films before and after cycles were examined on scanning electron microscopes (SEM, 6335F and TESCAN VEGA3). The elemental distribution was explored using energy dispersive spectrometers (EDS). X-ray photoelectron spectroscopy (XPS, PHI5600 by Physical Electronics, Inc.) was conducted using monochromatic Al Ka X-ray at 14 kV. Raman spectra were obtained on a Witec-Confocal Raman system (UHTS 600 SMFC VIS). The wettability of electrolyte on the surface of these block layers were measured using a goniometer

(Theta of Attension, Biolin Scientific) at room temperature. Electrical conductivity was measured on a four-probe resistivity/Hall system (HK5500PC, Bio-Rad).

2.3. Electrochemical tests

$V_2O_5 \cdot nH_2O$/CNT films were synthesized as the cathode for ZIBs. The preparation details and the XRD pattern of the electrode (Fig. S1) are described in *Supporting Information*. CR2032 coin cells were assembled in the ambient using Zn foil as the anode and $V_2O_5 \cdot nH_2O$/CNT as the cathode with a Ti foil as the current collector. 1 M $Zn(ClO_4)_2$ in H_2O was adopted as electrolyte. The block layer was inserted between the glass fiber separator (Whatman, GF/D) and the cathode. The coin cells without and with different films were charge/discharge cycled between 0.2 and 1.6 V on a LAND 2001 CT battery tester. The electrochemical impedance spectra (EIS) were obtained at a constant perturbation amplitude of 5 mV in the frequency range between 0.01 Hz and 100k Hz on a VMP electrochemical workstation (Biologic, France) at room temperature.

3. Results and discussion

The morphology of the rGO film was characterized by SEM (Fig. 1b and 1c), showing a flat surface and a layered structure through the entire cross-section where the thickness is ~2 μm. The XPS analysis was employed to investigate the chemical compositions and the presence of functional groups in different films, as shown in Fig.

1d. In the deconvoluted C 1s spectra, two prominent peaks located at ~284.6 and ~285.2 eV are attributed to C=C and C-C, respectively. Four other peaks at ~286.1, ~287.2, ~288.0 and ~288.9 eV arise from the functional groups, C-OH, C=O=C, C=O and O=C-OH, respectively [17]. The C/O ratio gradually increases from 1.8/1.0 in the pristine GO to 17.3/1.0 for 1000rGO, as a reflection of an enhanced reduction degree. Raman spectra of GO and rGO films are shown in Fig. 1e. The two peaks at ~1350 and ~1599 cm^{-1} correspond to D- and G-bands. The down-shift of G-band of rGO films results from the recovery of hexagonal network of carbon atoms with defects [21]. The increase of the I_D/I_G intensity ratio from 0.83 of GO to 1.02 of 1000rGO suggest the decrease of the average size of sp^2 domains upon the removal of most oxygenated functional groups [22, 23]. Before utilizing as a block layer, the electrolyte wettability was evaluated by measuring the contact angles of the same amount of electrolyte applied on GO and rGO films (Fig. 1f). The contact angle of the electrolyte on GO is 54°. Along with the increase of reduction temperature, the contact angles climb to 64°, 74° and 80° for 350rGO, 600rGO and 1000rGO, respectively. The increasing contact angle indicates a decreasing wettability due to the removal of oxygenated functional groups.

The GO and rGO films were assembled between the separator and the cathode in ZIBs. To examine the insertion of block layer on the internal resistance, the electrochemical impedance spectra (EIS) were obtained before cycles as shown in Fig.

2a. The characteristic impedance parameters were fitted by the equivalent circuit where R_e refers to the resistance of electrolyte; R_{ct} represents the kinetic resistance of charge transfer at the electrode/electrolyte interface or intrinsic charge transfer resistance of the electrodes; and W_0 is the diffusion resistance. All the data are summarized in Table S1. It is noted that the cell with a GO film presents a highest R_{ct} value of 258.3 Ω, which is not surprised as GO film has very low conductivity in the order of 10^{-4} S/cm. R_{ct} decreases with increasing reduction temperature. The value for the cell having rGO100 block layer is even lower than the one without the film, originating from the excellent conductivity of rGO films reduced at high temperatures. A six-order improvement of conductivity has been observed after thermal reduction at 1000 ℃ compared to pristine GO film, as shown in Table S2.

The voltage profiles of the cells without and with block layers are given in Fig. 2b, which have similar shapes indicating the block layer does not affect the charge storage mechanism [24]. Fig. 2c exhibits the cyclic performance of the cells measured at a galvanostatic charge/discharge current of 100 mA g^{-1} between 0.2 and 1.6 V at room temperature. The cell without a block layer shows a very fast capacity degradation, remaining only 57 mAh g^{-1} after 50 cycles due to the instability and dissolution of active materials in the aqueous electrolyte. The dissolved active materials are probably $V_{10}O_{27}(OH)^{5-}$ ions according to the previous report [25]. A conventional cathode via

slurry coated on titanium foils also presents a fast capacity degradation, as shown in Fig.S2 After inserting a GO film, the battery presents much stable capacities and retains 182 mAh g^{-1} after 50 cycles, implying the inhibition of soluble V_2O_5 migration. It is worth noting the different initial capacities of the cells without and with the GO or rGO films may result from the irreversible reduction of GO (Fig. S3) and the irreversible oxidation of Zn anodes [7]. The cells with 350rGO and 600rGO exhibit much higher and more stable capacities of 283 and 298 mAh g^{-1} after 50 cycles, respectively. The improved capacities arise probably from the high conductivities of rGO films after reduction [24]. However, the battery with the 1000rGO film delivers a fast capacity degradation from its initial capacity of 411 mAh g^{-1} to only 159 mAh g^{-1}. It suggests the higher reduction degree of rGO film can enhance the capacity but deteriorate the stability. It is speculated that both the decreased wettability and densely stacked structure of 1000rGO decrease the electrolyte permeation and lower the ion transport through the film, which can be responsible for the poor performance [26, 27]. The capacity increases of cells with rGO films in initial cycles are due to the activation of active materials where dissolved active materials are prohibited from free diffusing to the anode and are fully utilized [20, 28]. The comparison of rate capabilities of these cells measured at increasing current rates from 0.1 to 2 A g^{-1} is given in Fig. 2d. The cell without the block layer delivers fast capacity decays at all the current rates. With

the GO film, the stability of the cell is improved but the capacities are very low. The capacities can be ignored at a high current density of 2 A g^{-1}, resulting from the low conductivity of the GO film. Among the films after reduction, the battery with 600rGO presents the optimal electrochemical behaviors, demonstrating the highest capacities of 415, 407, 333, 284 and 221 mAh g^{-1} at 0.1, 0.2, 0.5, 1 and 2 A g^{-1}, respectively. When the rate is reduced back to 0.5 and 0.1 A g^{-1}, the capacity still maintains 305 and 389 mAh g^{-1}, respectively. The long-term cyclic test of the cell with 600rGO was therefore measured at a high current density of 2 A g^{-1} as shown in Fig. 2e. A low current density of 100 mA g^{-1} was conducted to activate the active materials in the first five cycles. The battery remains 191 mAh g^{-1} after 500 cycles and the efficiencies constantly sustain around 100% during the cyclic process, evidencing its stable capability and excellent reversibility.

To investigate the mechanism of enhanced electrochemical performances of cells with block layers, the migration confinement of active materials was demonstrated using a simple setup shown in Fig. 3a. A small vial containing $V_2O_5 \cdot nH_2O$ dissolved electrolyte solution (in yellow color) was capped with a separator and a GO/rGO film. The vial was then upside-down placed inside a large vial filled with neat electrolyte. The color change of the electrolyte solution in the large bottle was monitored. It is revealed that the neat solutions with the pristine separator and the one with GO film

became light yellow after three days, indicating active materials within the smaller vial freely diffused through the separator and permeated the GO film. In contrast, the color of the solution with rGO films hardly changed, reflecting the rGO layer functions as an effective barrier to $V_2O_5 \cdot nH_2O$ diffusion. The effect of block layer in preventing the shuttle of active materials is further confirmed in the cycled cells. The cathode with rGO600 presents a more stable structure than the one without a block layer after the first discharge and charge cycle as examined by XRD in Fig. S4, where the electrode without a film shows a much lower crystallinity. Furthermore, the cells after 40 cycles were disassembled and examined. Without a block layer, the separator is eroded with brown deposits, whereas the one with 600rGO seems to be much clear as shown in Fig. S5. $V_2O_5 \cdot nH_2O$ nanowires are entangled with CNTs in the pristine electrode (Fig. S6). After cycling, the structure of $V_2O_5 \cdot nH_2O$ nanowires collapses in both cells with and without a rGO layer as a consequence of active material dissolution. Bare CNTs are observed in the cell without a block layer as part of $V_2O_5 \cdot nH_2O$ has migrated to the anode side (Fig. 3b). The EDS results of Zn anodes with and without a rGO600 film after 5 cycles are compared in Fig S7. 0.05 wt% vanadium element was detected for the anode with a block layer, much lower than the one without a film, indicative of the effective confinement of dissolved active materials freely migrating to the anode. Turning to the cathode with 600rGO (Fig. 3c and 3d), the nanowire structure also

collapses, but active materials remain intertwined with CNTs. It is also demonstrated by the mapping results showing uniform distribution of V and C elements. Since the dissolved active materials remain confined on the cathode side, exposed CNTs are rarely spotted.

One of the major concerns in the rGO interlayer is that it may be detrimental to the Zn ion transfer. The Zn ion transference numbers of cells without and with block layers were therefore compared using a potentiostatic polarization method [29, 30]. Zn-Zn symmetric cells were adopted. A sandwich composite, which was prepared with the block layer stacked between two glass fiber separators, was placed between the two Zn electrodes. A small constant potential of 10 mV was applied, and the Current (*i)*-time *(t)* curve was recorded. The current keeps decreasing in the first three hours and reaches a steady state afterward. The current contribution from the anions is excluded at steady state, thus enabling the calculation of cation transference number by the following equation [29, 30]:

$$t_+ = \frac{I_S(\Delta V - I_0 R_0)}{I_0(\Delta V - I_S R_S)} \quad (1)$$

Where I_s is the steady-state current, I_0 represents the initial current, ΔV refers to the applied potential. R_s and R_0 are the electrode resistances after and before the polarization, which was measured by EIS (Fig. 4). A very low transference number of 0.18 is obtained for the cell without rGO layer, signifying that severe migration of

dissolved species occurs, which contributes significantly to the initial current I_0. After inserting the 600rGO layer, the I_0 is much lower than the one without the layer. Accordingly, the transference number increases to 0.67. It suggests the block layer prevents only the migration of dissolved active materials but not the Zn ions. The enhanced Zn ion transport is probably due to a large amount of sp^2 clusters on all stacking rGO layers connect together to form a sp^2 nanocapillary network, providing a rapid Zn ion pathway between cathodes and anodes [31]. The aforementioned electrolyte solution method, SEM observations and transference number measurements all demonstrate the optimized rGO layer confines the free diffusion of dissolved active materials to the anode and facilitates the Zn ion transport, so as to enhance the stability and capability of aqueous ZIBs, as schematically illustrated in Fig. 4c.

The shuttle of active materials always leads to fast self-discharge, which afflicts the aqueous batteries [32]. The protective interlayer is expected to alleviate this phenomenon. The self-discharge behaviors of the cells were then evaluated. The batteries were cycled at 500 mA g^{-1} for 20 cycles and then rested for 72 h before further discharging, as shown in Fig. 5 and Fig. S8. The battery without an interlayer releases only a 33% capacity of the 20th charged value, corresponding to a fast self-discharge rate of 0.93% per hour. The reason lies in the dissolution of active materials and their shuttling to the anode as discussed before. In contrast, self-discharge is largely

mitigated with a 600rGO block layer. A 88% discharge capacity to the charged one is recovered, corresponding to a low self-discharge rate of 0.17% per hour thanks to the suppression of the shuttle effect.

Another issue plaguing aqueous batteries is the poor performance at low temperatures. Most conventional aqueous electrolytes are liable to freeze at a temperature below 0 ºC, discouraging the charge transfer [33]. To study the environmental stability, the cells with 600rGO were evaluated at subzero temperatures. As shown in Fig. 6, the cell cycled at 0 ºC show identical voltage profiles at the 50th cycle as those at room temperature. This suggests the same phase transition process during Zn insertion/extraction. The capacity is decreased to 276 mAh/g at the 2nd cycle at 0 ºC due to the slow Zn ion transfer. Nevertheless, excellent cyclic stability is maintained and a capacity of 277 mAh/g is retained after 100 cycles. In comparison, the neat cathode shows a rapid capacity degradation at 0 ºC (Fig. S9), as a result of active materials dissolution as described before. It should be mentioned that the electrolyte remains a liquid state at 0 ºC due to the drop in the freezing point in the presence of salt [34]. The performance is further examined at an extremely low temperature of -20 ºC. The charge/discharge curves at -20 ºC present a larger overpotential, because of higher Ohmic and kinetic overvoltages at the extremely low temperature. Although the electrolyte becomes solid at -20 □, ions can transport with a

much higher internal resistance (Fig. S10). A decent capacity of 106 mAh/g is gained after 100 cycles with superior cyclic stability. It further demonstrates the importance of the rGO layer in confining the free diffusion of active materials and facilitating the charging transfer at both room and low temperatures.

4. Conclusions

A freestanding rGO film is prepared and explored as a block layer in ZIBs. Effect of the oxygenated functional groups is systematically studied, which have considerable influence on the wettability, conductivity, and permeability of the block layer. The block layer utilizing optimal rGO film effectively prevents the migration of dissolved active materials, while allows the free diffusion of Zn ions. As a result, the battery with 600rGO delivers a high reversible capacity of 191 mAh g^{-1} after 500 cycles at 2 A g^{-1} and bears a much-reduced self-discharge rate at room temperature. Application-wise, the temperature behavior of ZIBs is also investigated. The assistance of rGO interlayer enables a decent performance at the low temperatures of 0 and -20 ℃.

Acknowledgments

This work was financially supported by the Hong Kong Polytechnic University [Grant 1-ZE83; Area of Excellence Project 1-ZE30].

References

[1] H. Kim, J. Hong, K.Y. Park, H. Kim, S.W. Kim, K. Kang. Chem. Rev. 114(23) (2014)11788-11827.

[2] J. Muldoon, C.B. Bucur, T. Gregory. Chem. Rev. 114(2014)11683-11720.

[3] C. Pan, R. Zhang, R.G. Nuzzo, A.A. Gewirth. Adv. Energy Mater. 8(2018)1800589.

[4] D. Kundu, B.D. Adams, V. Duffort, S.H. Vajargah, L.F. Nazar. Nat. Energy 1(2016)16119.

[5] C. Xia, J. Guo, Y. Lei, H. Liang, C. Zhao, H.N. Alshareef. Adv. Mater. 30(2018)1705580.

[6] C. Xu, B. Li, H. Du, F. Kang. Angew. Chem. Int. Ed. 51(2012)933-935.

[7] H. Pan, Y. Shao, P. Yan, Y. Cheng, K.S. Han, Z. Nie, C. Wang, J. Yang, X. Li, P. Bhattacharya, K.T. Mueller, J. Liu. Nat. Energy 1(5)(2016)16039.

[8] S. Zhao, B. Han, D. Zhang, Q. Huang, L. Xiao, L. Chen, D.G. Ivey, Y. Deng, W. We. ACS Appl. Mater. Interfaces 10(2018)24573−24582.

[9] L. Zhang, L. Chen, X. Zhou, Z. Liu. Adv. Energy Mater. 5(2015)1400930.

[10] Z. Liu, G. Pulletikurthi, F. Endres. ACS Appl. Mater. Interfaces 8(2016)12158-12164.

[11] P. He, M. Yan, G. Zhang, R. Sun, L. Chen, Q. An, L. Mai. Adv. Energy Mater.

7(11)(2017)1601920.

[12] X. Dai, F. Wan, L. Zhang, H. Cao, Z. Niu. Energy Storage Mater. 17(2019)143-150.

[13] X. Chen, L. Wang, H. Li, F. Cheng, J. Chen. J. Energy Chem. 38(2019)20-25.

[14] F. Hu, D. Xie, D. Zhao, G. Song, K. Zhu. J. Energy Chem. 38(2019)185-191.

[15] B. Wu, G. Zhang, M. Yan, T. Xiong, P. He, L. He, X. Xu, L. Mai. Small 14(13)(2018)1703850.

[16] D. Xu, H. Wang, F. Li, Z. Guan, R. Wang, B. He, Y. Gong, X. Hu. Adv. Mater. Interfaces 6(2018)1801506.

[17] S. Islam, M. H. Alfaruqi, J. Song, S. Kim, D.T. Pham, J. Jo, S. Kim, V. Mathew, J.P. Baboo, Z. Xiu, J. Kim. J. Energy Chem. 26(2017)815-819.

[18] J.Q. Huang, X. Guo, X. Lin, Y. Zhu, B. Zhang. Hybrid aqueous/organic electrolytes enable the high-performance Zn-ion batteries. Submitted.

[19] Y. Geng, S.J. Wang, J.K. Kim. J. Colloid Interf. Sci. 336(2)(2009)592-598.

[20] J.Q. Huang, Z.L. Xu, S. Abouali, M. Akbari Garakani, J.K. Kim. Carbon 99(2016)624-632.

[21] K. Krishnamoorthy, M. Veerapandian, R. Mohan, S.J. Kim. Appl. Phy. A 106(3)(2012)501-506.

[22] Y. Fang, R. Hu, B. Liu, Y. Zhang, K. Zhu, J. yan, K. Ye, K. Cheng, G. Wang, D.

Cao. J. Mater. Chem. A 7 (10)(2019)5363-5372.

[23] S. Fang, D. Huang, R. Lv, Y. Bai, Z.H. Huang, J. Gu, F. Kang. RSC Adv. 7(2017)25773-25779.

[24] J.Q. Huang, B. Zhang, Z.L. Xu, S. Abouali, M. Akbari Garakani, J. Huang, J.K. Kim. J. Power Sources 285(2015)43-50.

[25] J. Livage. Chem. Mater. 2(1991)578-593.

[26] X. Lin, X. Shen, Q. Zheng, N. Yousefi, L. Ye, Y.W. Mai, J.K. Kim. ACS Nano 6(2012)10708-10719.

[27] K.H. Thebo, X. Qian, Q. Zhang, L. Chen, H.M. Cheng, W. Ren. Nat. Commun. 9(2018)1486.

[28] X. Wang, Z. Wang, L. Chen. J. Power Sources 242(2013)65-69.

[29] V. Mauroa, A. D'Apranoa, F. Croceb, M. Salomonc. J. Power Sources 141(2005)167–170.

[30] S. Zugmann, M. Fleischmann. M. Amereller. R.M. Gschwind, H.D. Wiemhöfer, H.J. Gores. Electrochim. Acta 56(2011)3926-3933.

[21] J.Q. Huang, T.Z. Zhuang, Q. Zhang, H.J. Peng, C.M. Chen, F. Wei. ACS Nano 9 (3)(2015)3002-3011.

[32] M. Pasta, C.D. Wessells, R.A. Huggins, Y. Cui. Nat. Commun. 3(2012)1149.

[33] S.S. Zhang, K. Xu, T.R. Jow. J. Power Sources 115(1)(2003)137-140.

[34] A. Ramanujapuram, G. Yushin. Adv. Energy Mater. 8(35)(2018)1802624.

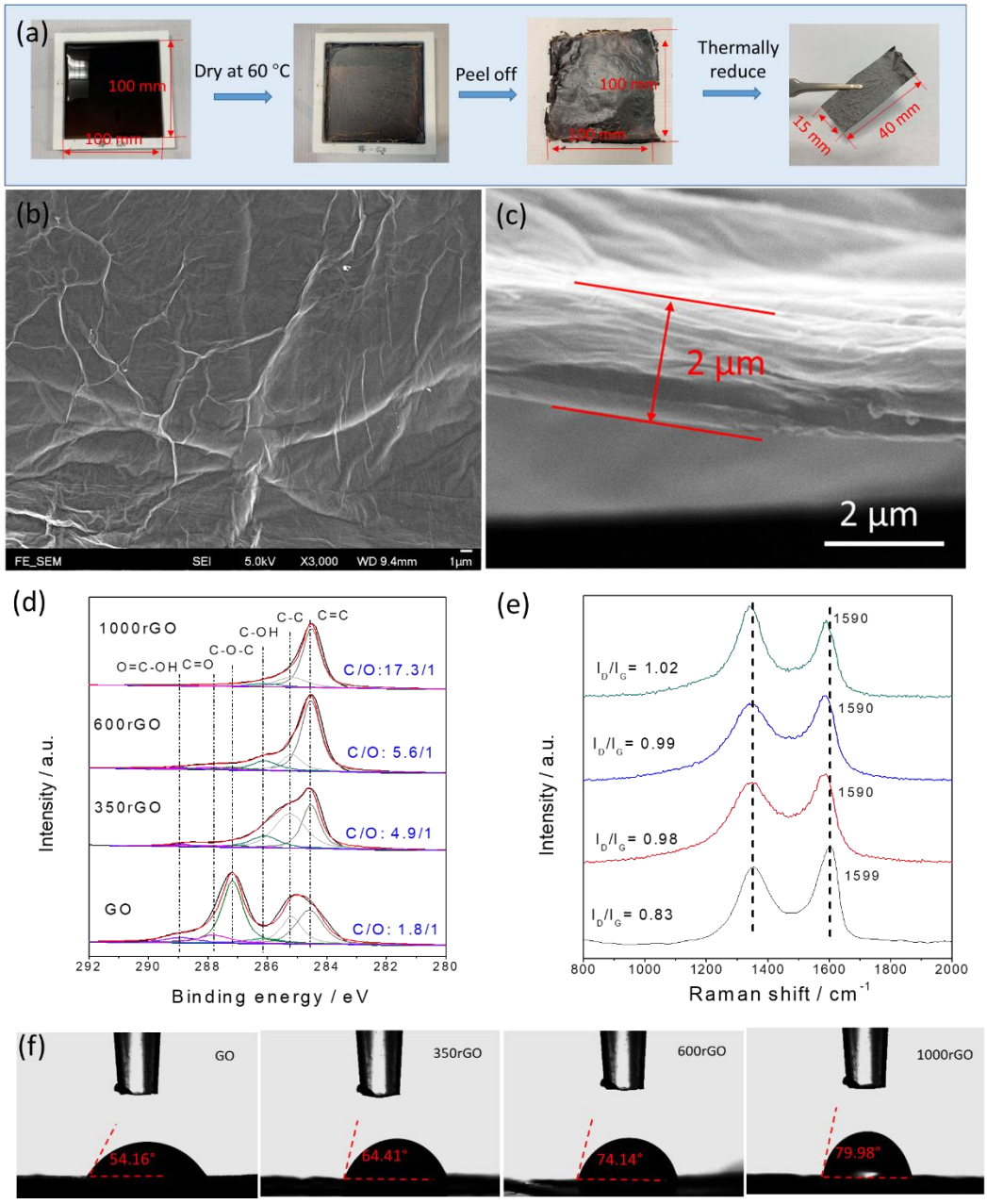

Fig. 1 (a) Schematic of preparation of rGO block layers; SEM images of (b) top surface and (c) cross-section of 600rGO films; (d) XPS deconvoluted C 1s spectra and (e) Raman spectra of GO and rGO films; (f) comparison of electrolyte wettability on GO, 350rGO, 600rGO and 1000rGO films.

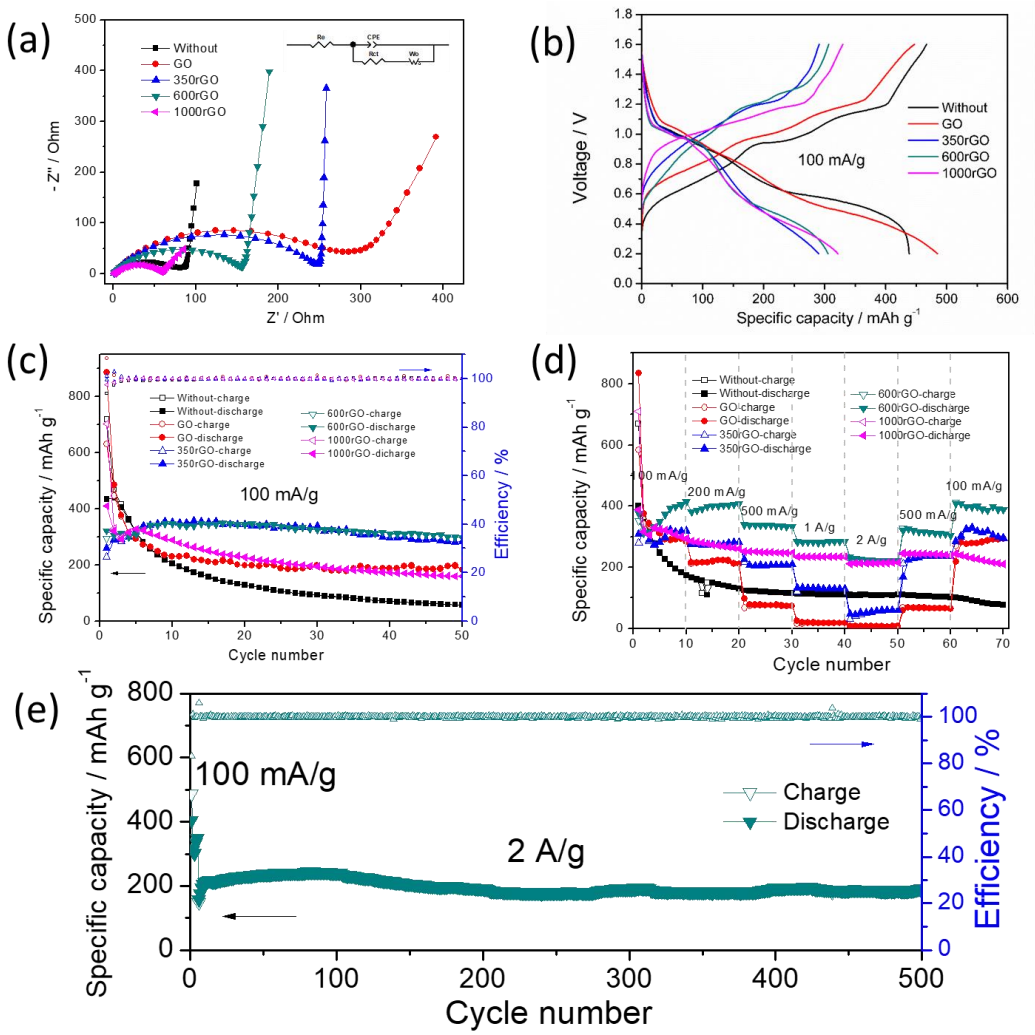

Fig. 2 (a) EIS with the equivalent circuit in the inset, (b) discharge and charge curves in the 2nd cycle, (c) cyclic performance and (d) rate capability of ZIBs without and with GO and rGO films; (e) long-term cyclic performance of the ZIBs with a 600rGO film at 2 A g^{-1} at room temperature.

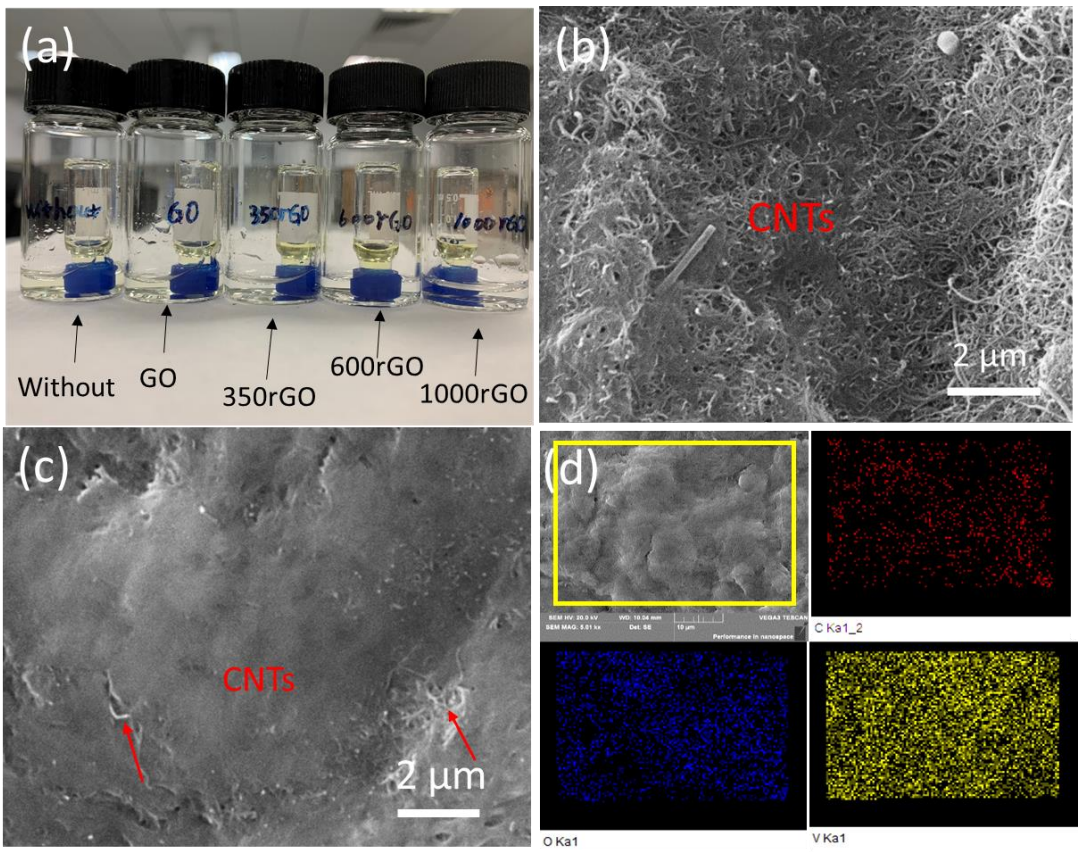

Fig. 3 (a) $V_2O_5 \cdot nH_2O$ diffusion behaviors of pristine separator and separators with block layers; SEM images of cathodes (b) without and (c) with 600rGO after 40 cycles; (d) SEM elemental maps of the cathode with 600rGO after 40 cycles.

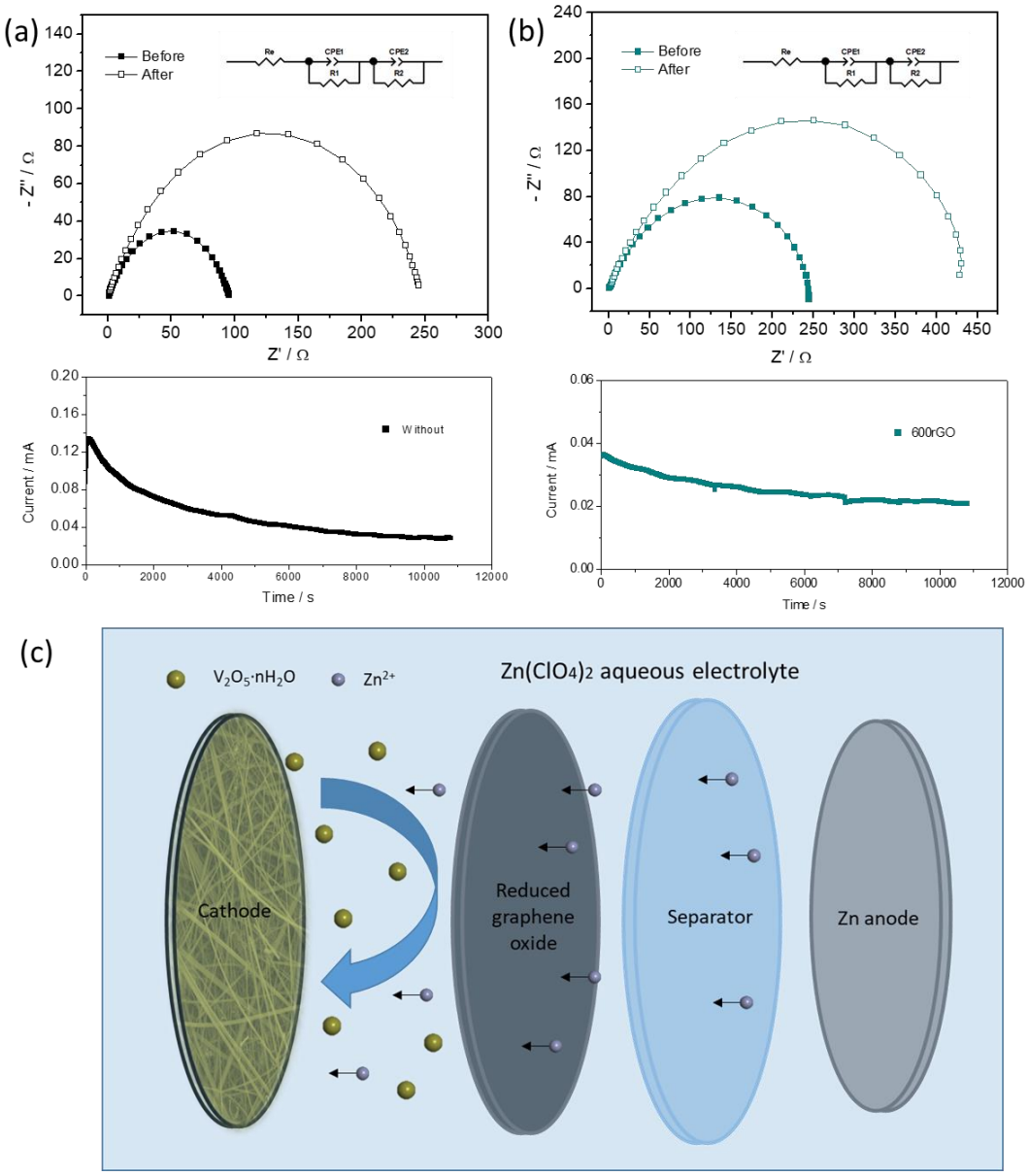

Fig. 4 The potentiostatic polarization of ZIBs. EIS and polarization curves of cells (a) without block layer and (b) rGO600 before and after polarization; (c) schematic of $V_2O_5 \cdot nH_2O$ migration behavior with a rGO film.

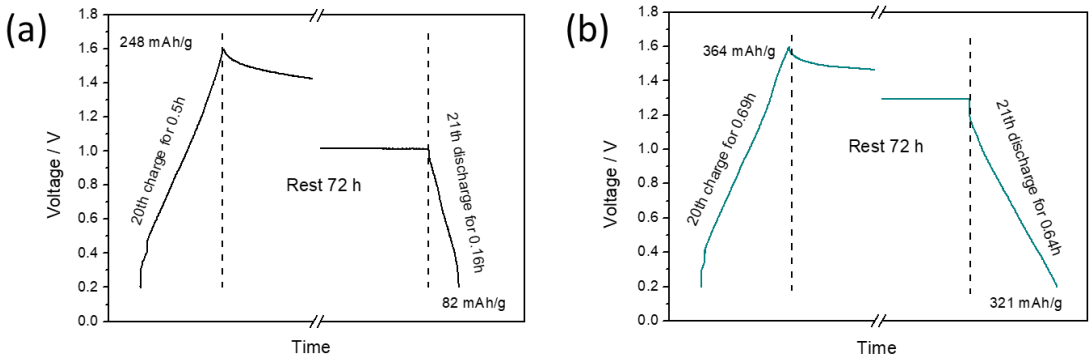

Fig. 5 Self-discharge performance of ZIBs (a) without and with (b) 600rGO films.

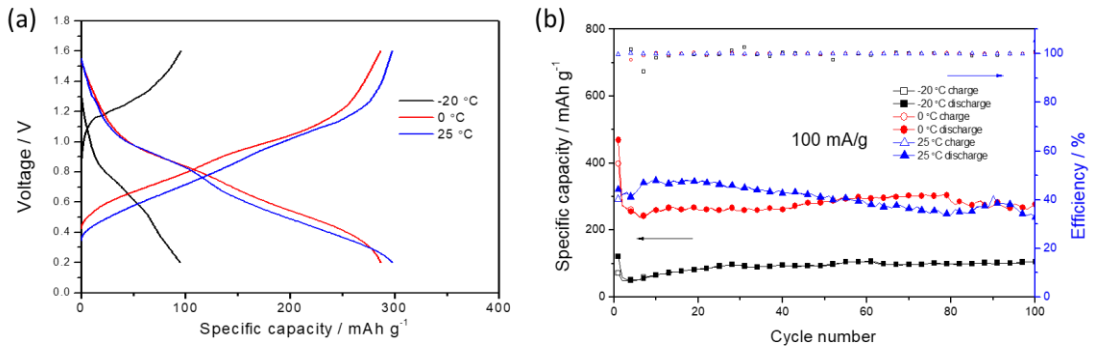

Fig. 6 (a) Voltage profiles of the 50th cycle; (b) cyclic performance of ZIBs with 600rGO films at different temperatures.